XX IMEKO World Congress
Metrology for Green Growth
September 9–14, 2012, Busan, Republic of Korea

AUTOMATED CLOUD BASE HEIGHT AND WIND SPEED MEASUREMENT USING CONSUMER DIGITAL CAMERAS

Fernando M. Janeiro[1], *Filipe Carretas*[2], *Konrad Kandler*[3], *Pedro M. Ramos*[4] *and Frank Wagner*[5]

[1]Universidade de Évora, Centro de Geofísica de Évora, Instituto de Telecomunicações, Évora, Portugal, fmtj@uevora.pt
[2]Universidade de Évora, Centro de Geofísica de Évora, Évora, Portugal, fcarretas@uevora.pt
[3]Institut für Angewandte Geowissenschaften, Technische Universität Darmstadt, 64287, Germany, kzk@gmx.de
[4]Instituto Superior Técnico, Instituto de Telecomunicações, Lisboa, Portugal, pedro.m.ramos@ist.utl.pt
[5]Universidade de Évora, Centro de Geofísica de Évora, Évora, Portugal, frankwagner@uevora.pt

Abstract: Cloud base height is an important parameter for climate studies as well as aviation safety. Ceilometers or LIDARs can measure this parameter but are usually expensive instruments. In this paper, a low-cost method to measure cloud base height based on consumer digital cameras and stereophotogrammetry is presented. The performance of the system is evaluated by comparison with LIDAR measurements. It is shown that the prototype can also measure the wind speed and direction at cloud height.

Keywords: Cloud height; Wind speed and direction; Stereo vision; Digital photography; Air safety.

1. INTRODUCTION

Clouds play a crucial role in the Earth's radiation budget and in the transport of water, thus affecting the global climate and the hydrological cycle [1]. Regular observations by national weather services report cloud type, approximate height and cover. Information on cloud base can be obtained by ground-based instruments such as radars [2] or laser based instruments such as ceilometers [3, 4] or LIDAR [5]. With increasing demand on regional or even local weather information, meteorological forecast models require better spatially resolved data. Therefore, low-cost automated observation systems are needed. A low-cost system will also benefit small aerodromes which usually cannot afford the instruments available at major airports. These aerodromes typically operate under Visual Flight Rules (VFR), where the minimum cloud height for which aircrafts can be operated has to be strictly enforced [6] due to safety issues.

A system based on two digital cameras with wide angle lenses has been developed to map cloud cover and cloud base height [7]. Recently, stereophotogrammetry with fish-eye lenses has been used to measure cloud level wind fields [8]. The preliminary results of a lower cost, consumer camera based, system for cloud height measurements have been presented in [9, 10].

This paper describes a permanently installed prototype that can measure cloud height, wind speed and wind direction with-low cost consumer digital cameras, therefore at a fraction of the price of the previously developed systems. The camera system calibration does not require laboratory facilities, since it is done on-site using stars. The algorithms for image registration [11] are also detailed in this paper. The system is fully automated and continuously reports the cloud base height and wind speed direction at cloud base. Measurements are compared with LIDAR data and meteorological model data [12] for validation of the system.

2. MEASUREMEN SYSTEM

2.1 Working Principle

Measurement of cloud base height can be performed by triangulation. By using two digital consumer cameras placed at a certain distance from each other, stereo vision can be used to perform the triangulation needed to measure the cloud height. Fig. 1 presents the geometry of the system where the two cameras L and R are pointing upwards and placed at a distance *d* from each other. An identifiable feature in a cloud (point C) needs to be visible from both cameras. The cloud height can be obtained from the measurement of the angles α_1 and α_2, through

$$h = \frac{\cos(\alpha_1)\cos(\alpha_2)}{\sin(\alpha_1 + \alpha_2)} d \,. \tag{1}$$

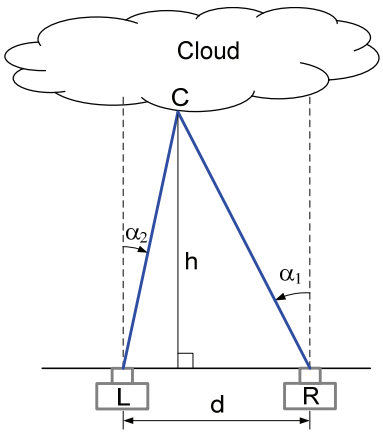

Fig. 1 – System geometry for the measurement of cloud base height through triangulation.

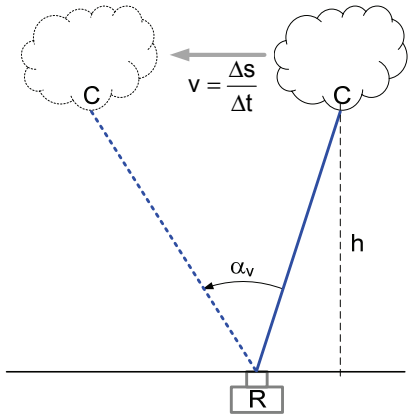

Fig. 2 – System geometry for wind speed measurement.

The wind speed and direction is measured by identifying the same feature in a cloud with a time-lapse Δt, as shown in Fig. 2. The measured angle α_w allows an estimation of the distance travelled by the cloud $\Delta s \simeq \alpha_w h$. Wind direction can also be obtained from the orientation of angle α_w relative to the camera coordinate system.

2.2 System Description

The installed prototype is composed by two DSLR cameras CANON EOS 1000D, a computer and an in-house developed triggering system based on a NI USB-6009 acquisition board. Each camera is enclosed in a box that provides weather protection as shown in Fig. 3. The two cameras are placed at a distance d = 28.9 m and are connected to a computer by USB cables with repeaters to overcome the 5 m limitation of the USB. These USB connections are used to download the photos to the computer for real time processing.

Fig. 3 – Camera weather protection box and overview of the prototype installation.

The cameras are set to take JPEG photos with resolution $L = 3888 \times W = 2592$. The zoom is set to minimum leading to a horizontal angle of view $\alpha_h = 64.5º$ and a vertical angle of view $\alpha_v = 45.5º$. The camera shutter can be remotely triggered by short-circuiting two input lines of the remote released socket input of the camera. The simultaneous triggering of the two cameras is accomplished by computer controlling the trigger. A LabVIEW program controls a data acquisition board by periodically sending 5 V pulses on one of its digital output channels that feeds a basic transistor switch. To take a picture, the switch creates a brief connection on the input lines of the camera. Tests have shown that the two cameras trigger at most within 1 ms of each other.

2.3 Camera System Calibration

The need for camera calibration arises from the difficulty in aligning the two cameras. The three most important factors in the camera misalignment are presented in Fig. 4. The misalignment shown in the front view manifests itself as displacement in the x direction of the cameras reference frame. Similarly, the misalignment represented in the side view will appear in the photos as a displacement in the y direction. The misalignment shown in top view will manifest itself as a rotation around the z axis of the camera reference frame.

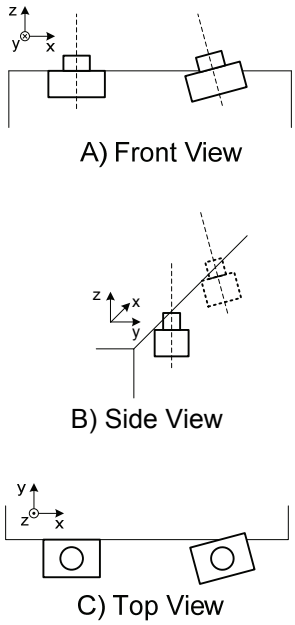

Fig. 4 – Types of misalignments: A) in x-axis of the camera; B) in y-axis of the camera; C) rotation about the z-axis.

A perfect alignment of the camera system is practically impossible. Therefore, it is more convenient to perform an approximate alignment and then determine the amount of misalignment in the system and correct for the remaining misalignment by software. The misalignment and consequently the calibration parameters can be obtained by taking simultaneous photos of the night sky when stars are visible.

Fig. 5 shows night photos from both cameras along with six stars chosen as control points. The chosen stars lie near the center of the photos to avoid the effect of barrel distortion which is always present in wide angle situations. The control points are used to extract the affine transformation (*i.e.*, translation and rotation) to match the two photos. The x and y translation corresponds to misalignments A and B of Fig. 4, while the rotation is the result of the misalignment in Fig. 4C.

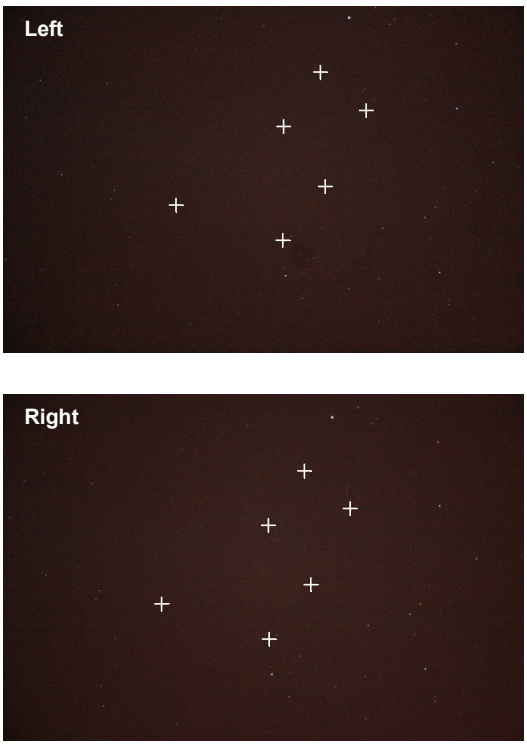

Fig. 5 – Night sky photos from left and right cameras with select stars as control points (white crosses). Images captured at 00:11 on January 17, 2012.

The affine transformation matrix for the case in Fig. 5 is

$$T = \begin{bmatrix} 0.9973 & -0.0095 & 0 \\ 0.0095 & 0.9973 & 0 \\ -117.93 & 104.25 & 1 \end{bmatrix}. \qquad (2)$$

Elements T_{31} and T_{32} correspond to the translation (in number of pixels) needed by the left photo to correct for the misalignments in Fig. 4A and Fig. 4B, respectively. These translations correspond to misalignment angles $\theta_x = -1.96°$ and $\theta_y = 1.83°$. From elements T_{11} and T_{21}, a rotation angle $\theta = 0.55°$ is found which corrects the misalignment shown in Fig. 4C.

Matrix T will be applied to the cloud photos from the left camera to compensate for the cameras misalignments shown in Fig. 4. In this way, the left camera photos will be transformed into the right camera's reference frame even though the cameras are only approximately aligned.

2.4 Image Registration

The determination of the cloud base height relies on the measurement of the angles α_1 and α_2 shown in Fig. 1. The procedure consists on simultaneously acquiring a cloud photo from each camera and then transforming the left image to compensate for the cameras misalignment, as previously described. Fig. 6 shows the transformed left photo as well as the right photo. It can be seen that the left photo has been translated to the left and bottom and has also been slightly rotated counterclockwise. The normalized cross correlation is applied to the cropped regions of the two photos, shown in red in Fig. 6. The resulting surface is shown in Fig. 7 and the coordinates of the maximum cross correlation give the offset $(\Delta x; \Delta y) = (-68; 6)$ of the left image relative to the right image.

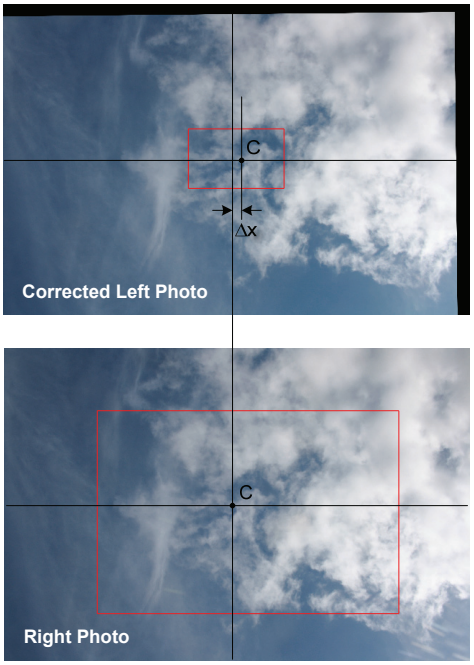

Fig. 6 – Image from the left camera (translated and rotated according to the calibration matrix) and image from right camera. Crops for normalized cross correlation shown in red.

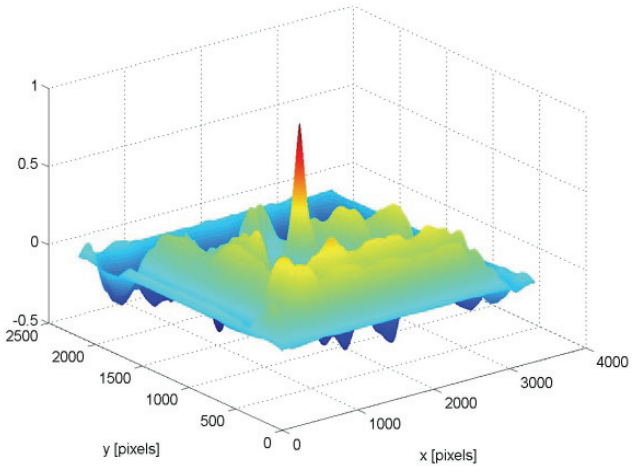

Fig. 7 – Normalized cross correlation between the photos shown in Fig. 6. The peak value yields the offset $(\Delta x; \Delta y)=(-68; 6)$ needed to overlay the two photos.

Due to the previous calibration stage, Δy should be zero and Δx should be completely attributed to the different viewing locations of the two photos. However, there is an uncertainty associated with matrix T, as well as with the normalized cross correlation procedure since the two photos have slightly different perspectives of the same cloud, thus explaining the Δy value.

Although the algorithm attempts to maximize the cross correlation between the central regions of the left and right photos, it can be considered that the recognized feature C is located at the center of the right image thus leading to $\alpha_1 = 0$. The angle α_2 is obtained from the Δx offset through

$$\alpha_2 = -\frac{\alpha_h}{L}\Delta x \tag{3}$$

from which the cloud height can be estimated.

Similarly, to determine the wind speed it is necessary to measure the angle α_w. In this case, two time-lapse photos with Δt = 19 s are acquired from the same camera. The normalized cross correlation yields an offset (Δx; Δy) which occurs because the clouds moved in the time-lapse between the two photos. The velocity of the cloud base level is obtained in the x and y directions of the camera reference frame through

$$v_x \simeq \left(\frac{\Delta x}{L}\alpha_h\right)\frac{h}{\Delta t},\ v_y \simeq \left(\frac{\Delta y}{W}\alpha_v\right)\frac{h}{\Delta t}. \tag{4}$$

The velocity magnitude and direction can then be obtained by

$$v = \sqrt{v_x^2 + v_y^2},\ \mathrm{dir}_{geo} = \mathrm{atan}\left(\frac{v_y}{v_x}\right) - \alpha_{geo} \tag{5}$$

where α_{geo} is the angle of the cameras base line relative to the geographical North as shown in Fig. 8.

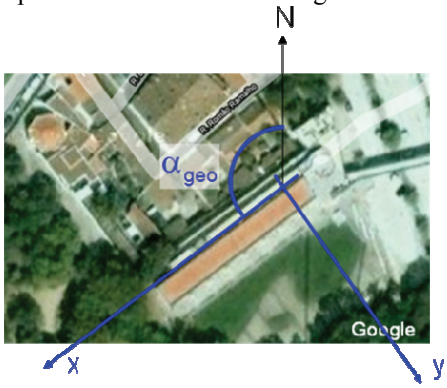

Fig. 8 – Cameras location and positioning relative to geographical North.

A necessary condition for estimating the wind speed and wind direction is that the clouds don't change their appearance. A long time lapse between 2 images improves the accuracy of the estimation (due to the higher number of pixels involved) but also increases the probability that the cloud shape changes. Measurements taken within 19 s are a good compromise between both effects.

3. MEASUREMENT RESULTS

The described prototype is installed in Centro de Geofísica de Évora (CGE) facilities and is measuring the cloud base height and wind speed and direction at cloud height. The measurements presented in this section were performed on 26 January 2012. The measured cloud height is compared with measurements from the LIDAR operated by CGE. The wind speed and direction are compared with meteorological data obtained from "READY – Air Resources Laboratory" website [12].

The cloud base height measured by the stereo vision cameras is shown in Fig. 9 by black dots which overlay the LIDAR measurements where warm colors represent the clouds detected by the LIDAR. Two layers of clouds were detected: a lower layer at around 1500 m and a higher layer at around 6000 m. The stereo vision system manages to measure the height of both layers with a somewhat good agreement with the LIDAR data. However, when both cloud layers are present in the photos, the systems yields a cloud height that has an intermediate value between the heights of the two layers. This behavior occurs because the image registration algorithm tries to register both layers, thus finding a compromise that results in an offset corresponding to an intermediate cloud height.

The resolution of the measured cloud height dramatically decreases as the cloud height increases due to the small angles involved and the limited pixel resolution of the photos. This effect is clearly seen in the measurement of the higher level clouds, where the resolution is about 350 m. This problem can be reduced by increasing the distance between the two cameras. However, this is not an issue in aerodrome applications since the interest lies on lower level clouds (up to 1200 m) where the resolution of the current camera system is better than 15 m.

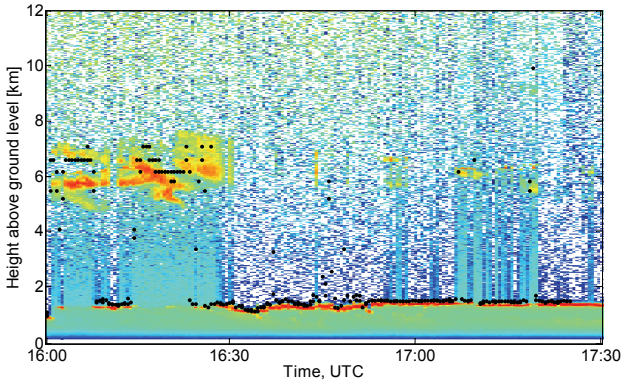

Fig. 9 – Cloud height measurements from stereo vision cameras (black dots). Color coded range corrected LIDAR signal. Warm colors represent the clouds detected by LIDAR measurements.

The measured wind speed is shown in Fig. 10 while the wind direction is presented in Fig. 11. The black dots show the wind parameter for the lower layer of clouds, while the red dots give the result of the higher cloud layer. The READY meteorological results [12], for two different times and for the heights closer to the two cloud layers are also shown in Fig. 10 and Fig. 11, showing good agreement with the measured values.

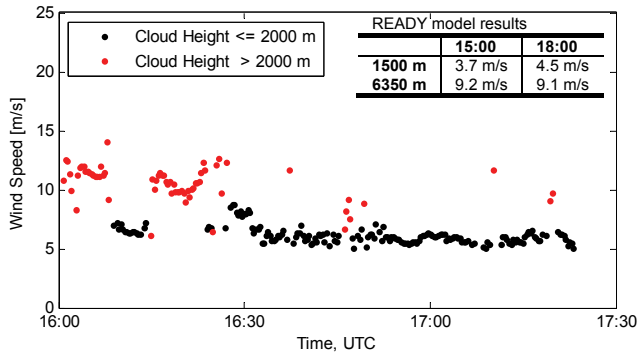

Fig. 10 – Wind speed measured by time-lapse photography for low clouds (black dots) and high clouds (red dots). Inset table presents the READY model results [12].

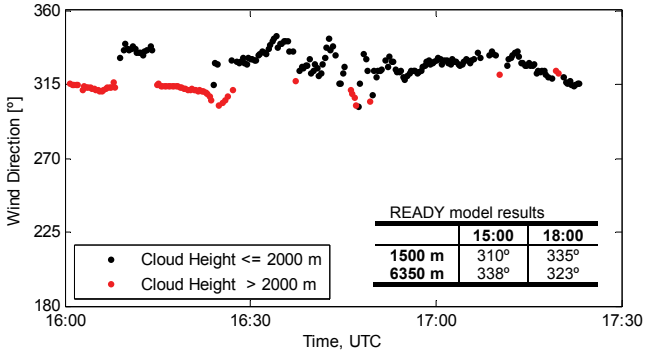

Fig. 11 – Wind direction measured by time-lapse photography for low clouds (black dots) and high clouds (red dots). Inset table presents the READY model results [12].

4. CONCLUSIONS

A low-cost camera system for the measurement of cloud base height and wind speed and direction at cloud base, based on stereophotogrammetry, has been implemented. This paper describes the current state of development of the prototype detailing the system setup and the algorithms used to calibrate and perform the measurements. Calibration of the cameras relative positions has been achieved by using stars in the night sky. The measurements do not require user intervention due to the use of image registration algorithms. Comparison with LIDAR data (for cloud height) and with available models (for wind speed and direction) validate the measurements performed by the camera system.

The resolution of the measured cloud height can be improved by increasing the cameras distance but at the cost of increasing the minimum height at which clouds are visible by both cameras. A possible solution might consist on installing a third camera at a longer distance, thus providing higher resolution measurements for higher clouds while maintaining the visibility of lower clouds. However, the current system is already well-suited for aerodrome deployment since, for flight operations, the main interest consists on determining the height of low level clouds.

ACKNOWLEDGMENTS

This work was supported by
FCT project PTDC/CTE-ATM/115833/2009
and Program COMPETE FCOMP-01-0124-FEDER-014508

REFERENCES

[1] *Climate Change 2007: The Physical Science Basis*, Contribution of Working Group I to the Fourth Assessment Report of the IPCC.

[2] J. H. Hand "Cloud Layer Detection by WSR-57 Radar", Journal of Applied Meteorology, vol. 3, pp. 58-64, 1964.

[3] J. L. Gaumet, J. C. Heinrich, M. Cluzeau, P. Pierrard, and J. Prieur, "Cloud-Base Height Measurements with a Single-Pulse Erbium-Glass Laser Ceilometer", Journal of Atmospheric and Oceanic Tech., vol. 15, pp. 37-45, 1998.

[4] Giovanni Martucci, Conor Milroy, Colin D. O'Dowd "Detection of Cloud-Base Height Using Jenoptik CHM15K and Vaisala CL31 Ceilometers", Journal of Atmospheric and Oceanic Technology, vol. 27, pp. 305-318, 2010.

[5] W. L. Eberhard "Cloud Signals from Lidar and Rotating Beam Ceilometer Compared with Pilot Ceiling", Journal of Atmospheric and Oceanic Tech., vol. 3, pp. 499-512, 1986.

[6] 14 CFR 91.155, "Basic VFR weather minimums" *Federal Aviation Regulations*, pp. 721–722, November 2010.

[7] G. Seiz, E. P. Baltsavias, A. Gruen, "Cloud Mapping from the Ground: Use of Photogrammetric Methods", Photogrammetric Engineerinf & Rmote Sensing, vol. 68, no. 9, pp. 941-951, September 2002.

[8] J. N. Porter, G. X. Cao, "Using Ground-Based Stereo Cameras to Derive Cloud-Level Wind Fields", Optics Letters, vol. 34, no. 16, pp. 2384-2386, August 2009.

[9] F. M. Janeiro, F. Wagner, P. M. Ramos, A. M. Silva, "Uncertainty Analysis of a Cloud Base Height Measurement System Based on Digital Photography", 3rd IMEKO TC19 International Symposium, Slovakia, September 2010.

[10] F. M. Janeiro, P. M. Ramos, F. Wagner, A. M. Silva, "Developments of Low-Cost Procedure to Estimate Cloud Base Height Based on a Digital Camera", Measurement, vol.43, no. 5, pp. 684-689, June 2010.

[11] J.C. Russ, The Image Processing Handbook, 5th ed., CRC Press, 2008.

[12] NOAA Air Resources Laboratory – READY (HYSPLIT) (http://ready.arl.noaa.gov/hysplit.php)